

Angle Locking of a Levitating Diamond using Spin-Diamagnetism

M. Perdriat, P. Huillery, C. Pellet-Mary, G. Hétet¹
¹*Laboratoire De Physique de l'École Normale Supérieure,
 École Normale Supérieure, PSL Research University,
 CNRS, Sorbonne Université, Université de Paris,
 24 rue Lhomond, 75231 Paris Cedex 05, France*

The negatively charged nitrogen-vacancy (NV) center in nano- or micro- diamonds has emerged as a promising magnetic field sensor [1, 2], as a candidate for hyper-polarizing paramagnetic species [3–5], as well as a tool for spin-mechanics at the nanoscale [6–9]. However, NV-doped diamonds are presently not straightforwardly employable for these applications in a liquid or when levitating under atmospheric pressures due to the random angular Brownian motion which tends to rotate the NV quantization axis [11–13] over the course of the measurements. Here, we report on angle locking of the crystalline axis of a trapped micro-diamond along an external magnetic field. Specifically, we use spin population inversion after a ground state level crossing of the NV center to turn the diamond into a diamagnet. The diamond crystalline axis naturally aligns to the magnetic field with high precision and in the absence of micro-wave, offering bright prospects for applications in biology and spin-mechanical platforms [14–16].

The current interest in the negatively charged nitrogen-vacancy center undoubtedly resides in the possibility to polarize and read out its electronic spin at ambient conditions [17]. Although the vast majority of experiments use photoluminescence to read-out the spin state, another tool was recently developed which makes use of the mechanical detection of magnetic-resonance with trapped diamonds [18], similar to in Magnetic-Resonance-Force-Microscopy (MRFM) [19]. It was shown that the diamond orientation held in position by electrostatic torques, could be deviated slightly from its equilibrium position using microwave induced torques across the NV centers spin resonances. The technique was further employed to cool the libration of the levitating diamond under vacuum [18] and to detect dipolar interactions between NV centers [10]. Here, we show that, after the ground state level anti-crossing (GSLAC) of the NV centers, the doped-diamond behaves as a material with a strong magnetic anisotropy and turns into a diamagnet. We then use the spin-diamagnetism to confine the orientation of a trapped micro-diamond along the applied magnetic field at ambient conditions.

In a general anisotropic magnetic material with a tensor magnetic susceptibility $\underline{\underline{\chi}}$, the mean magnetization per unit volume is related to the magnetic field \mathbf{H} by the relation $\mathbf{M} = \underline{\underline{\chi}}\mathbf{H}$. Assuming rotational symmetry about the hard axis, the magnetic torque applied to the material is then given by $\boldsymbol{\tau} = \mu_0 V \mathbf{M} \times \mathbf{H} = \mu_0 V \Delta \chi (\mathbf{n} \times \mathbf{H}_\perp) H_\parallel$, where $\Delta \chi = \chi_\parallel - \chi_\perp$ is the difference between the susceptibility along the easy and hard magnetization axes. μ_0 is the free space magnetic permeability and V is the volume of the particle. \mathbf{n} is a unit vector along the hard magnetization axis. If $\Delta \chi$ is negative (resp. positive), the material is diamagnetic (resp. paramagnetic) and the torque tends to rotate the particle so that the easy axis of magnetization is perpendicular (resp. aligned to) the magnetic field [20, 21].

Let us now consider the magnetic response of the

negatively charged NV center in the absence of micro-wave. The ground electronic state of the NV[−] center is a triplet state with a zero-field splitting D due to magnetic dipole-dipole interaction between the two unpaired electrons [17]. One important feature of the NV[−] centers is that green laser light can polarize the electronic spin in the $|m_s = 0\rangle$ state [17]. In the absence of magnetic field, the other $|m_s = \pm 1\rangle$ states are degenerate and lie $D = (2\pi)2.87$ GHz above the $|m_s = 0\rangle$ state at room temperature. This interaction sets a natural quantization axis along the N-V direction shown in the Fig.1-a). The essence of the NV magnetism that we employ here lies in the $|m_s\rangle$ state mixing occurring in the presence of a magnetic field component that is perpendicular to the NV axis. Such state mixing generates a magnetic moment perpendicular to the NV axis, similar to in van Vleck paramagnetism [20]. To quantify this, we consider first a single class of NV centers with a density $d = N/V \approx 1\text{ppm}$ of NV centers that are polarized in the ground state. In the limit $\gamma_e H/\mu_0 \ll D$, where γ_e is the electron gyromagnetic ratio, we find

$$\Delta \chi \approx d \mu_0 \hbar \frac{2\gamma_e^2}{D} \approx 10^{-4} > 0. \quad (1)$$

In this regime, the NV-doped diamond features anisotropic paramagnetism with an easy axis of magnetization that is perpendicular to the NV axis. Including the four NV centers orientations along the four [111] diamond crystalline axes, one finds that the total susceptibility drops to about 10^{-5} . The four NV classes thus give rise to a net torque that averages out spatially to give a value of the order of the diamond orbital diamagnetism ($\Delta \chi_{\text{orb}}^{\text{max}} \approx 10^{-5}$) in all directions [10]. By pushing the magnetic field up to a regime where $\gamma_e H/\mu_0 \approx D$, only the states $|m_s = 0\rangle$ and $|m_s = -1\rangle$ mix significantly so that

$$\mathbf{M}_\perp \approx d \mu_0 \hbar \frac{\gamma_e^2 \Delta}{\Delta^2 + (\Gamma_2^*)^2} \mathbf{H}_\perp, \quad (2)$$

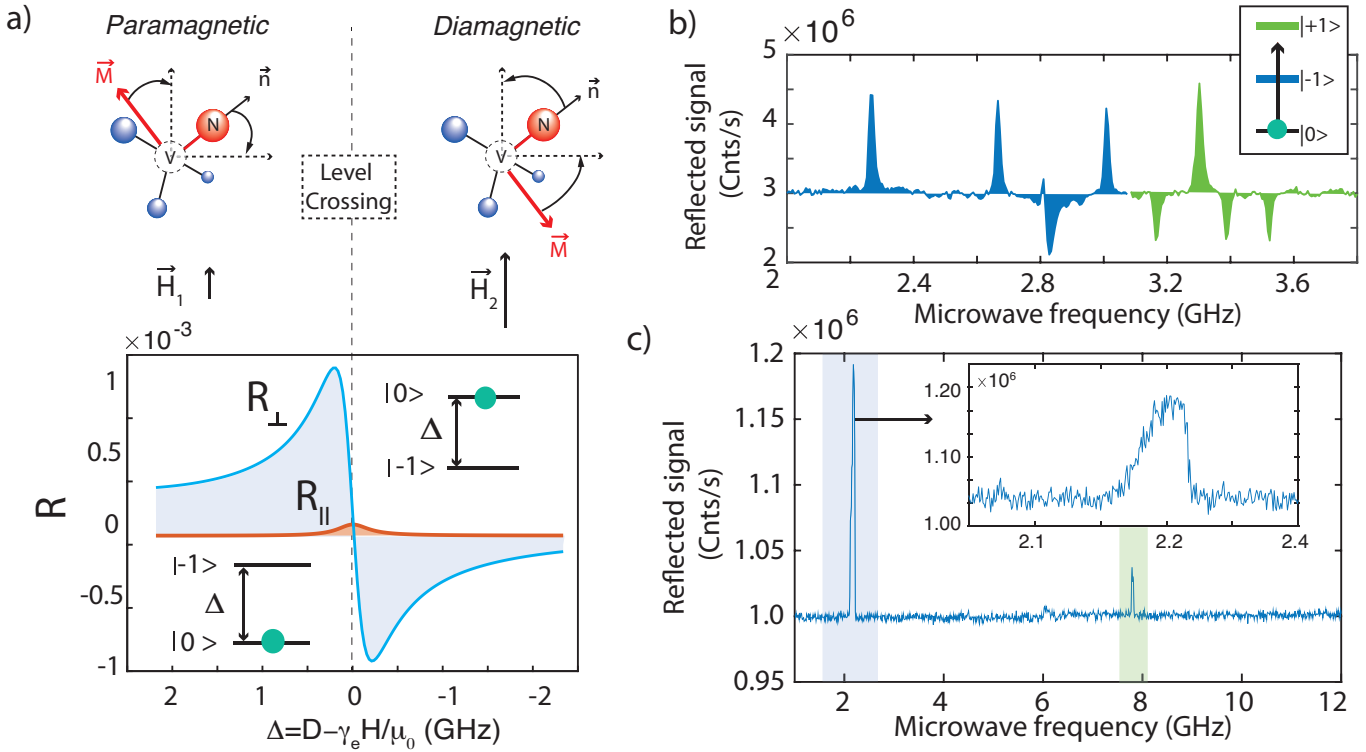


FIG. 1. **Magnetic response of the NV-doped diamond across a para/diamagnetic transition.** a) Calculated ratios R_{\perp} (resp. R_{\parallel}) between the induced NV magnetization and the magnetic field as a function of $D - \gamma_e H / \mu_0$ close to one [111] crystalline direction in blue (resp. red) line. b) and c) are Torque-detected-magnetic-resonances taken in the para- (resp.) dia-magnetic regimes. The inset of c) is a zoom on the first transition at 2.2 GHz.

when \mathbf{n} is close to the magnetic field axis. Here $\Gamma_2^*/2\pi \approx 5$ MHz is the spin dephasing rate due to the fluctuating dipolar coupling to substitutional nitrogen atoms and $\Delta = D - \gamma_e H / \mu_0$ (See SI). Importantly, when $\Delta < 0$, the NV spins are in the first excited state. The NV optically excited state intersystem crossing preserves polarization in the $|m_s\rangle \approx |0\rangle$ state even after the GSLAC which can result in a population inversion, as in the recently demonstrated diamond maser [22]. For this reason, here, the induced magnetization is opposed to (diamagnet) or is parallel to (paramagnet) the applied magnetic field, depending on the sign of Δ , as indicated by Eq. 2. Further, the dia- or para- magnetism is predicted to be much larger in magnitude than in the $\gamma_e H / \mu_0 \ll D$ paramagnetic regime. This is shown in Fig. 1-a) where the ratio R between the induced magnetization and the applied magnetic field is plotted as a function of Δ for an angle $\theta = 10$ mrad between \mathbf{H} and \mathbf{n} , demonstrating two orders of magnitude larger magnetic response close to the GSLAC. $R_{\perp} = M_{\perp} / H_{\perp}$ (resp. $R_{\parallel} = M_{\parallel} / H_{\parallel}$) is shown by the blue (resp. red) line.

Experimentally, a micro-diamond particle with a concentration of NV centers between 3-5 ppm is loaded in an electrostatic trap (See Methods). In order to characterize the NV-induced magnetism, we continuously apply green laser light and sweep the frequency of a microwave sig-

nal far from the spin-transition saturation. This creates a small magnetization along \mathbf{n} when the microwave frequency coincides with an electronic spin resonance. At this resonance condition, the equilibrium angular position of the diamond given by trap restoring torque and the magnetic torque is slightly modified. The microwave scans give transient torques to the particle that enable tracking the angles of the four NV classes with respect to the applied magnetic field (see Methods).

One of the resulting spectra is plotted in Fig. 1-b) in the regime $\gamma_e H / \mu_0 \ll D$. We found that, here, the position of the four NV angles do not depend significantly on the applied magnetic field when varied from 0 to about 40 mT. The equilibrium angular position is thus largely determined by the electrostatic trap. A spectrum in the $\Delta < 0$ regime is shown in Fig. 1-c). Here, only two lines clearly detach from the spectra, with a very large signal to noise ratio. Importantly, their frequencies are consistent with an almost ideal alignment of one NV axis along the magnetic field (see Method), as expected from a diamagnetic response. Such spectra are observed in almost all of the particles, pointing towards a strong magneto-optical rotation of the particles in the trap. Another indication is given by a zoom on the $|m_s = 0\rangle$ to $|m_s = -1\rangle$. The blue-detuned sharp edge of the mechanical response, in the inset of Fig. 1-c), shows that removing population

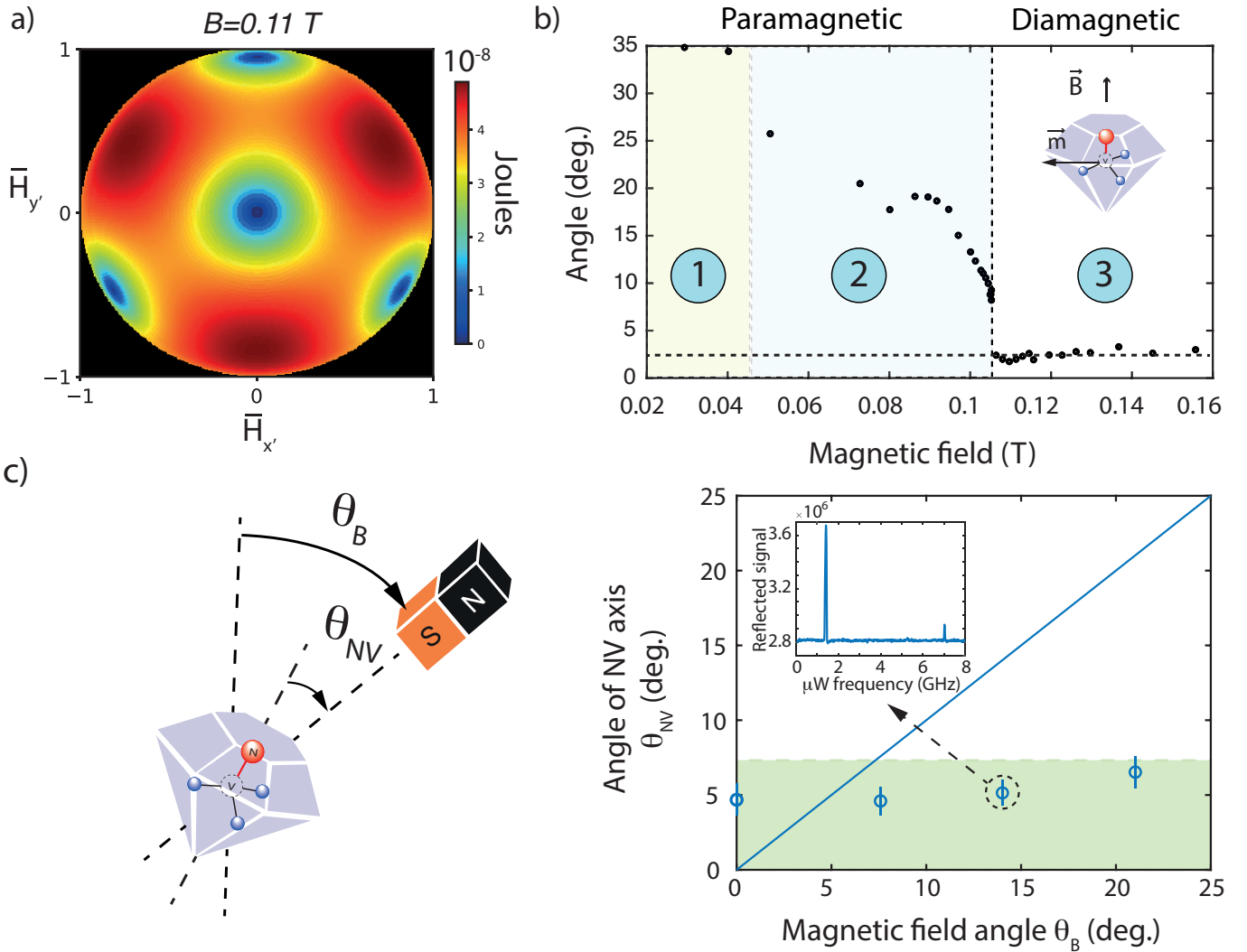


FIG. 2. **Mechanical response of the trapped diamond as a function of magnetic field amplitude and angle** a) Magnetic energy as a function the magnetic field directions with a diamond containing 10^9 NV centers. $\bar{H}_{x',y'} = H_{x',y'}/|\mathbf{H}|$, where x' and y' are the directions perpendicular to the central NV axis. b) Angle of one of the diamond [111] axis versus magnetic field amplitude. c) Angle of one of the diamond [111] axis versus magnetic field angle. Right: The plain blue line predicts a response obtained without NV induced magnetism. The inset is a mechanically-detected magnetic-resonance scan taken for the third magnetic field angle $\theta_B \approx 14$ degrees.

from the $|m_s \approx 0\rangle$ state misaligns the NV and magnetic field axes (see methods).

Numerical calculations of the magnetic energy of the NV centers as a function of the projections of the magnetic field with respect to the [111] direction are shown in Fig. 2-a). The four [111] directions of the NV centers are seen to be confining, with a potential depth that is three orders of magnitude larger than $kT \approx 10^{-21}$ J at $T=300$ K. Beyond the GSLAC we thus expect that the spins can indeed pull the [111] crystalline direction towards the magnetic field direction. In Fig. 5-b), we study the modification of the angle of the NV centers axis that is closer to the magnetic field axis as a function of the magnetic field amplitude (See Methods and extended data 1). Three regions can be identified. When

the magnetic field ranges from 0 to 45 mT (region 1), the angle of the diamond does not change significantly. When the magnetic fields ranges from 45 mT to 105 mT however, the angle reduces until it suddenly drops. The evolution of the angle in region (1) and (2) results from a competition between the torque applied by the Paul trap and by the other classes of NV centers (See Methods). Importantly, close to 105 mT, a sharp transition occurs where the angle between the NV centers and the magnetic field reaches $\approx 2^\circ$. The angle remains at this value over a wide range of magnetic fields. The change of the angle is thus consistent with the above described transition from a paramagnetic state to a diamagnetic state at the ground state level anti-crossing. The latter transition is expected to take place at $B=102.4$ mT,

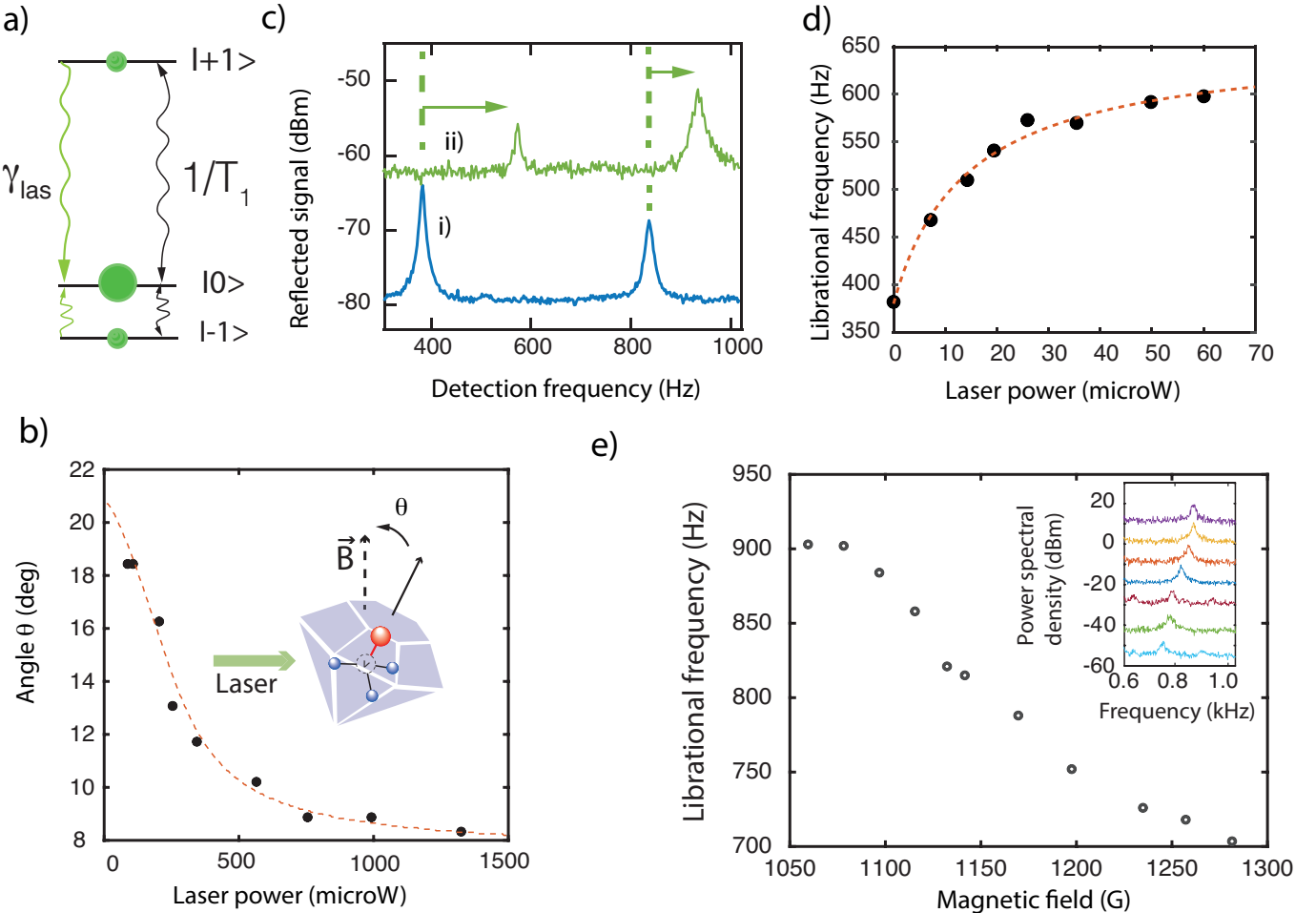


FIG. 3. Magneto-optical tuning of the mechanical response a) Eigenstates of the NV center’s electronic spins. Green arrows depicts optical pumping to the $|m_s = 0\rangle$ state and black arrows depict depolarizing mechanisms. b) Angle of one of the NV axes with respect to the magnetic field direction (as shown in the inset) as a function of the green laser power. c) trace i) resp. ii) show the power spectral density of the vibrational modes without/with the polarizing green laser respectively. d) Vibrational frequency as a function of laser power. e) Angular confinement characterized by the vibrational frequency, as a function of magnetic field. The inset shows the power spectral density of the mechanical oscillator for different B-field values.

which is very close to the observed critical B-field ($B_c \approx 105$ mT). Another check that firmly establishes NV spin induced diamagnetism is that the particle [111] direction follows the magnetic field direction. This is demonstrated in Fig. 2-c) where, as the magnetic field direction is rotated, the angle between the NV and magnetic field axis stays constant.

Using Eq. 2, one finds that the associated librational confinement $\omega_{\text{dia}}/2\pi$ is stronger than the Paul trap confinement in the diamagnetic region (3) (see Methods). The magnetic response is particularly enhanced by the laser induced spin-polarization (see Fig. 3-a)) which reduces the effective spin-temperature close to the μK . Fig. 3-b) shows that the NV axis can indeed be steered towards the magnetic field because of the laser induced decrease in the effective spin-temperature, similar to the Curie-Weiss law. The observed optically controlled magnetization of the doped diamond overwhelms the diamag-

netic contribution from the orbital motion of the electrons in the diamond. The librational frequency $\omega_{\text{dia}}/2\pi$ also increases with the laser power once in the region (3). To observe this effect, we operate the trap under vacuum (see Methods). Fig. 3-c) i and ii) show the power spectral density (PSD) of the librational modes without (i) and with (ii) the polarizing green laser. The dependence in the observed librational frequencies is plotted in Fig. 3-d), showing again the strong magneto-optical nature of the effect. The inset of Fig. 5-e) shows the PSD zoomed to one librational mode as a function of the magnetic field. The central frequency of this mode decreases as a function of the magnetic field as expected from Eq. (2).

Our observations opens up several new directions. Already now, the induced NV spin-magnetization is strong enough to contemplate observing the confining magnetic force from the NV centers, similar to what was achieved using the inherent diamond diamagnetism [23, 24]. Cal-

culations suggest that increasing the NV spin density by a factor of a 10 and working with purer samples will further enable reaching an internal magnetization that is of the order of the applied magnetic field. In the diamagnetic limit, the total internal magnetic field can be reduced significantly, opening prospects for levitating diamonds in a similar regime than with the Meissner effect in superconductors.

Being able to align diamond main crystalline axes along magnetic fields also means that they can more easily be employed for polarizing other spins, such as the nuclear spins of the ^{13}C atoms of molecules under liquid environments [3–5]. Many groups are currently working towards polarizing paramagnetic species in solution using the NV centers inside nanodiamonds [25]. One difficulty with current attempts is to achieve large NV polarization under the necessarily strong magnetic field required for cross-polarization. Our technique may thus enable counteracting one drawback, which is the lack of NV polarization in NDs in liquid due to uncontrolled NV angle, and thus boost the hyper-polarization efficiency [27].

More generally, our work may find applications for remote control of the motion of nano- or microscopic objects. Typically, the remote control of crystal motion is done purely optically [11], magnetically [28–30] or electrically, as in Microelectromechanical systems (MEMS). However, local remote control of the orientation of an object at the nanoscale is often difficult due to their small moment of inertia. The presented magneto-optical confinement offers a potential solution for stabilizing the angle of NDs in optical tweezers operating in liquid environments [11, 13] and for the many spin-mechanical schemes that require micro-wave free angular stabilization [7–9].

ACKNOWLEDGMENTS

We would like to thank L. Rondin, V. Jacques, A. Dréau and C. Voisin for fruitful discussions, as well as Ludovic Mayer for lending us microwave equipment. GH acknowledges SIRTEQ for funding.

[1] R. Schirhagl, K. Chang, M. Loretz, and C. L. Degen, *Annual Review of Physical Chemistry* **65**, 83 (2014).

[2] L. Rondin, J.-P. Tetienne, T. Hingant, J.-F. Roch, P. Maletinsky, and V. Jacques, *Reports on Progress in Physics* **77**, 056503 (2014).

[3] F. Shagieva, S. Zaiser, P. Neumann, D. B. R. Dasari, R. Stöhr, A. Denisenko, R. Reuter, C. A. Meriles, and J. Wrachtrup, *Nano Letters* **18**, 3731 (2018).

[4] D. A. Broadway, J.-P. Tetienne, A. Stacey, J. D. A. Wood, D. A. Simpson, L. T. Hall, and L. C. L. Hollenberg, *Nature Communications* **9**, 1246 (2018).

[5] P. Fernández-Acebal, O. Rosolio, J. Scheuer, C. Müller, S. Müller, S. Schmitt, L. P. McGuinness, I. Schwarz, Q. Chen, A. Retzker, B. Naydenov, F. Jelezko, and M. B. Plenio, *Nano Letters* **18**, 1882 (2018).

[6] S. Castelletto, L. Rosa, and A. Boretti, *Diamond and Related Materials* **106**, 107840 (2020).

[7] C. Wan, M. Scala, G. W. Morley, A. A. Rahman, H. Ulbricht, J. Bateman, P. F. Barker, S. Bose, and M. S. Kim, *Phys. Rev. Lett.* **117**, 143003 (2016).

[8] T. Delord, L. Nicolas, Y. Chassagneux, and G. Hétet, *Phys. Rev. A* **96**, 063810 (2017).

[9] Y. Ma, T. M. Hoang, M. Gong, T. Li, and Z.-q. Yin, *Phys. Rev. A* **96**, 023827 (2017).

[10] C. Pellet-Mary, P. Huillery, M. Perdriat, and G. Hétet, *Magnetic Torque Enhanced by Tunable Dipolar Interactions* ArXiv 01/03 (2021).

[11] M. Geiselmann, M. L. Juan, J. Renger, J. M. Say, L. J. Brown, F. J. G. de Abajo, F. Koppens, and R. Quidant, *Nat Nano* **8**, 175 (2013).

[12] L. P. Neukirch, E. von Haartman, J. M. Rosenholm, and N. VamivakasA., *Nat Photon* **9**, 653 (2015).

[13] V. R. Horowitz, B. J. Alemiøen, D. J. Christle, A. N. Cleland, and D. D. Awschalom, *Proceedings of the National Academy of Sciences* **109**, 13493 (2012).

[14] D. Lee, K. W. Lee, J. V. Cady, P. Ovartchaiyapong, and A. C. B. Jayich, *Journal of Optics* **19**, 033001 (2017).

[15] P. Rabl, P. Cappellaro, M. V. G. Dutt, L. Jiang, J. R. Maze, and M. D. Lukin, *Phys. Rev. B* **79**, 041302 (2009).

[16] M. Scala, M. S. Kim, G. W. Morley, P. F. Barker, and S. Bose, *Phys. Rev. Lett.* **111**, 180403 (2013).

[17] M. W. Doherty, N. B. Manson, P. Delaney, F. Jelezko, J. Wrachtrup, and L. C. L. Hollenberg, *Physics Reports* **528**, 1 (2013).

[18] T. Delord, P. Huillery, L. Nicolas, and G. Hétet, *Nature* **580**, 56 (2020).

[19] D. Rugar, R. Budakian, H. J. Mamin, and B. W. Chui, *Nature* **430**, 329 EP (2004).

[20] J. H. Van Vleck, *The theory of electric and magnetic susceptibilities* (Clarendon Press, 1932).

[21] R. L. Carlin, *Magnetochemistry* (Springer Science & Business Media, 2012).

[22] J. D. Breeze, E. Salvadori, J. Sathian, N. M. Alford, and C. W. M. Kay, *Nature* **555**, 493 (2018).

[23] J.-F. Hsu, P. Ji, C. W. Lewandowski, and B. D’Urso, *Scientific Reports* **6**, 30125 (2016).

[24] M. C. O’Brien, S. Dunn, J. E. Downes, and J. Twamley, *Applied Physics Letters* **114**, 053103 (2019).

[25] D. E. J. Waddington, M. Sarracanie, H. Zhang, N. Salameh, D. R. Glenn, E. Rej, T. Gaebel, T. Boele, R. L. Walsworth, D. J. Reilly, and M. S. Rosen, *Nature Communications* **8**, 15118 (2017).

[26] H.-J. Wang, C. S. Shin, C. E. Avalos, S. J. Seltzer, D. Budker, A. Pines, and V. S. Bajaj, *Nature Communications* **4**, 1940 (2013).

[27] J. P. Tetienne, L. T. Hall, A. J. Healey, G. A. L. White, M. A. Sani, F. Separovic, and L. C. L. Hollenberg, arXiv e-prints , arXiv:2008.12417 (2020), arXiv:2008.12417 [cond-mat.mes-hall].

[28] J. J. Abbott, E. Diller, and A. J. Petruska, *Annual Review of Control, Robotics, and Autonomous Systems* **3**, 57 (2020).

[29] C. Li, G. C. Lau, H. Yuan, A. Aggarwal, V. L. Dominguez, S. Liu, H. Sai, L. C. Palmer, N. A. Sather,

T. J. Pearson, D. E. Freedman, P. K. Amiri, M. O. de la Cruz, and S. I. Stupp, *Science Robotics* **5** (2020).

[30] J. A.-C. Liu, B. A. Evans, and J. B. Tracy, *Advanced Materials Technologies* **5**, 2000147 (2020).

EXTENDED DATA

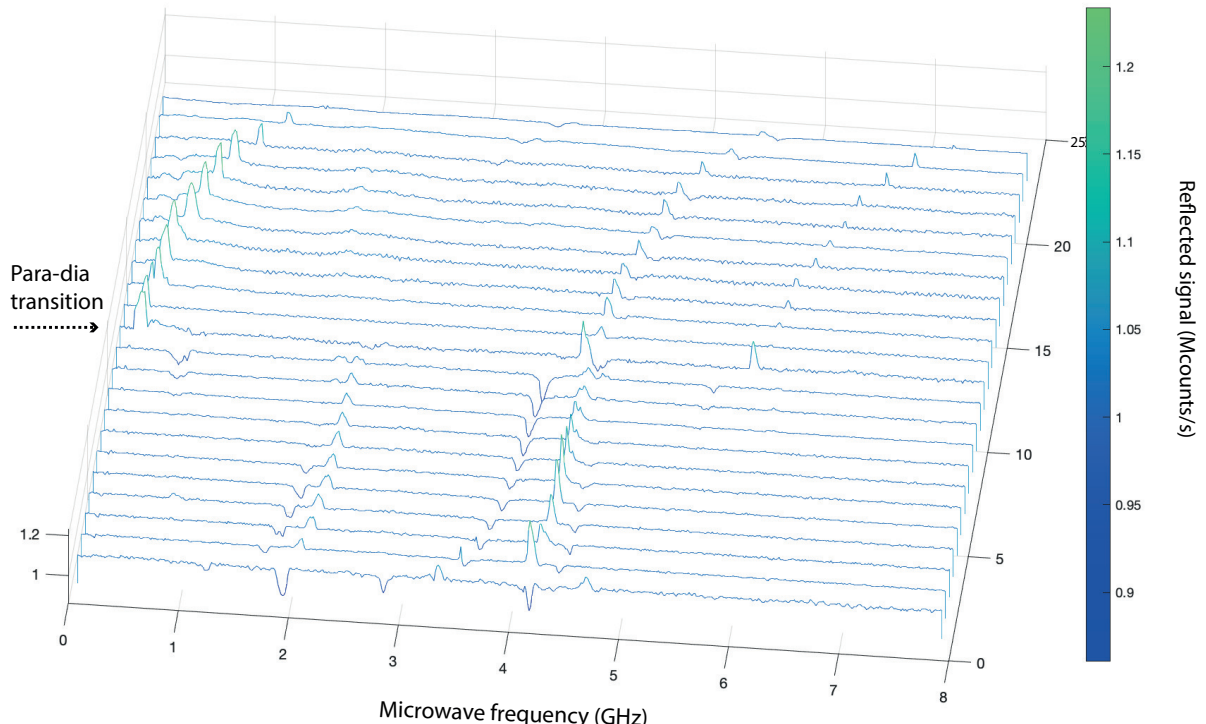


FIG. 4. Mechanically detected magnetic resonance curves for different magnetic field values. From the position 0 to 25 the magnetic field spans the range 0.03 to 0.16 mT. In the diamagnetic regime, one sees that the MDMR lines are equidistant because the diamond no longer rotates in this range of magnetic field values.

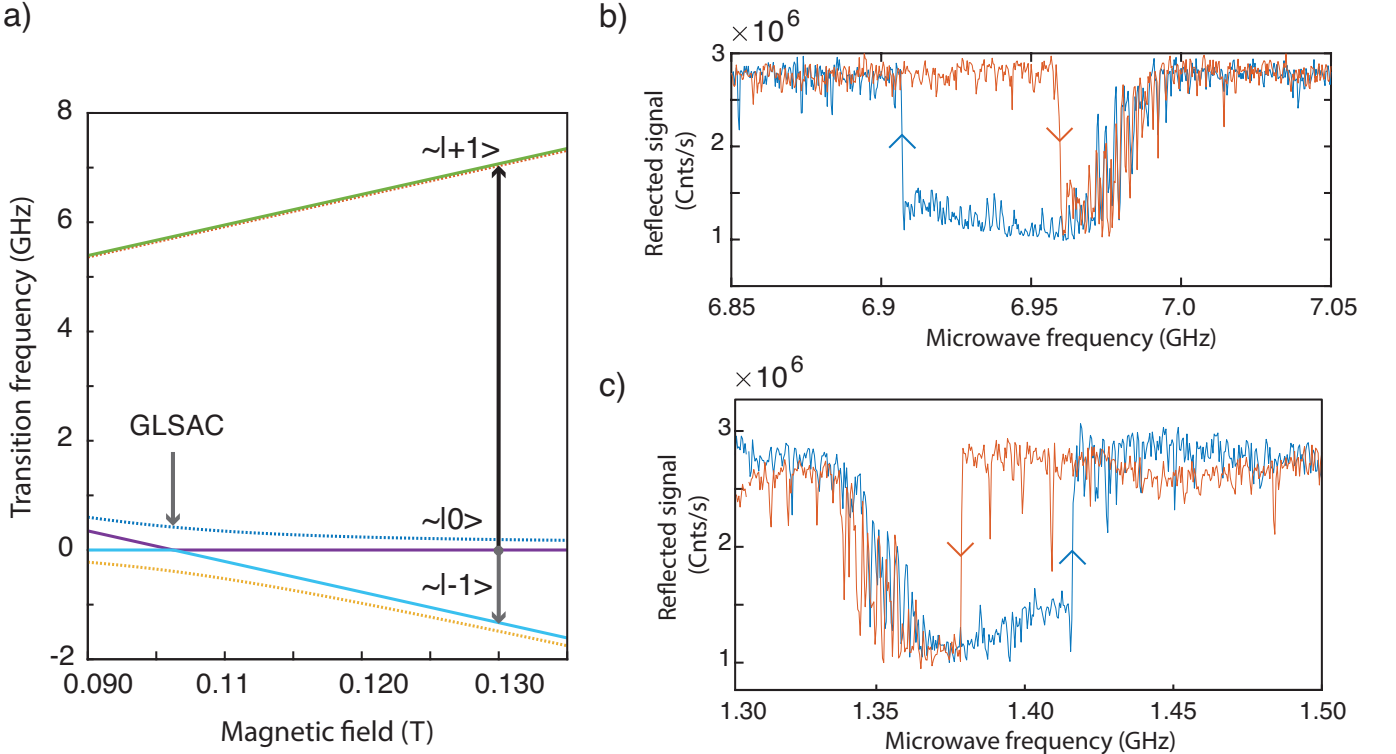


FIG. 5. a) Evolution of the energies of the three eigenstates in the range 0.09 to 0.135 T for 0.2 radians (dashed lines) and 0 radians (plain lines). b) Single shot (not averaged) MDMR in the non-linear regimes for the 0 to +1 transition when the microwave is scanned from the blue to the red side (blue curve) and from the red to the red side (red curve). When the +1 state is excited, the angle increases and the transition frequency decreases so the sharp edge is on the red side. c) Single shot MDMR in the non-linear regimes for the 0 to -1 transition. Similar color code as in b). Here, when the -1 state is excited, the angle increases and the transition frequency increases so the sharp edge is on the blue side.

METHODS

NV and Paul trap parameters The experiment is similar to the one used in [1]. The diamond sample was bought from the company Adamas and contains ≈ 5 ppm of nitrogen-vacancy centers. The green laser is focused by an objective with a numerical aperture of 0.5. The photo-luminescence (PL) is collected by the same objective, separated from the excitation light using a dichroic mirror and a 532nm notch filter, and detected using a multimode-fiber single-photon avalanche photo-detector (SPCM-AQRH-15 from Perkin Elmer). The objective is slightly defocused in order to illuminate the whole diamond. The Paul trap is a ring Paul-Straubel trap with a diameter of approximately 200 μm . It acts both as a trap through the high voltage (HV) and as a microwave (MW) antenna. The Paul trap provides angular confinement with librational frequencies ranging from 100 Hz to 1 KHz, depending on the particle shape, size, total surface charges.

Due to an intersystem crossing in the excited state of the NV⁻ center, the electronic spin can be polarized in the $|m_s = 0\rangle$ state [2]. Under typical laser powers, we can polarize the NV spins to the $|m_s = 0\rangle$ state with an efficiency above 50%. Due to dipolar interactions amongst

the spins, the longitudinal spin-relaxation rate Γ_1 was measured to be ≈ 2 kHz. The dephasing rate $\Gamma_2^* = 5$ MHz, is mostly due to the coupling between the NV centers and the bath of nitrogen spins (so called P_1 centers). The laser polarization rate ranges from 10 to 1000 kHz depending in the position of the lens with respect to the diamond and depending on the density of NV centers at the focal point of the laser [1] due to the aforementioned dipolar processes.

Mechanically-Detected-Magnetic-Resonance. In Mechanically-Detected-Magnetic-Resonance (MDMR) measurements, a microwave resonantly excites the electronic spins of the NV centers, thereby slightly rotating the diamond. Starting from the laser polarized state $|m_s = 0\rangle$, a microwave creates a net magnetization whose amplitude does not depend on the magnetic field.

The diamond motion is detected by collecting the back reflected light from the diamond interface, while scanning the microwave signal. To detect the diamond motion, we focus a small area of the reflected signal onto an optical fibre and detect the photons transmitted through the fibre with a single-photon avalanche photodiode. Compared to the experiment performed in [1], we use of an extra laser at 747 nm in order to read-out the angular motion while

not impacting the spin-state. This means that the Paul trap angular motion can be estimated without the spin torque. Using this detection method, motional frequencies can be observed by sending the detected signal to a spectrum analyzer. Under vacuum (1 mbar), the power spectral density (PSD) exhibits narrow peaks at the motional frequencies which are driven by the collisions with the background gaz (Brownian motion).

Thanks to the very high spin-torques and the high sensitivity of the speckle detection [1], the microwave current enters the Paul trap wire without pre-amplification in these measurements. The microwave power that is employed is around -10 to 0 dBm, as measured before the trap. Importantly, only the magnetization component along \mathbf{n} couples to the angular degree of freedom during microwave excitation. The other transverse components of the spin operator oscillate at a frequency greater than 100 MHz, which is 5 orders of magnitude larger than the librational frequency. It thus has no direct impact on the libration.

NV Angle and magnetic field read-out The magnetic field amplitude as well as the angle θ of the NV centers with respect to the B field were estimated using NV magnetometry. Recording the frequency of two spectral lines ($\nu_{0,-1}, \nu_{0,+1}$) from the same NV class is enough to estimate both θ for this NV class as well as the magnitude of \mathbf{B} . This is done by diagonalizing the hamiltonian of the NV electronic spin. The transitions energy between the eigenstates is evaluated numerically for different angles and magnetic fields and one pair of transition frequency ($\nu_{0,-1}, \nu_{0,+1}$) can then be associated to one pair (θ, B) [3]. The width of the MDMR peaks varies from 5 to 20 MHz under weak microwave driving, which translates to errors in the determination of the angle of about 1 degree.

In regions 1 and 2 of Fig. 2 b), the evolution of the angle with respect to the B field results from a competitions between the torque applied by the Paul trap on the diamond and the other classes of NV centers. The characteristic librational frequencies of the Paul trap are 500 Hz - 1kHz. In the region 1, the paramagnetic susceptibility is $\approx 10^{-5}$ implies anti-confinement frequencies that are in the Hz range at these B field values, which is too small to make the spin-torque counteract the Paul trap confinement. In region 2 the paramagnetic susceptibility is large enough to displace the angle however (see Supplementary material for a theoretical analysis of the transition form region 2 to 3).

Reversed bistability Before the GSLAC, in the $| -1 \rangle$ resp. $| +1 \rangle$ states, the NV electronic spin states seek low transition frequencies because the spin torque tends to align/anti-align the NV centers to the B field. A consequence of this is that, in the non-linear regime, the sharp edge of the MDMR always appears on the red side [1]. In contrast, after the GSLAC, the spins are already aligned to the magnetic field due to the spin-induced diamagnetism, implying a modified non-linear MDMR response. The calculation of the energies of the new spin states

$|\pm\rangle$ close to the GSLAC is presented in the supplementary materials and in the extended data Fig. 2-a). The transverse component of the magnetic field generates an avoided crossing between the bare eigenstates of the \hat{S}_z' operator. At sufficiently large laser power and in the dispersive limit (see SI), the intersystem crossing in the optically excited state however polarizes the NV centers in the ground state before the GSLAC and in the second excited state after the GSLAC. When the NV centers are in the $|+\rangle$ state after the GSLAC, the spin-mechanical energy is confining.

The situation reverses in the presence of a microwave drive on the $|+\rangle$ to $|-\rangle$ transition. After the GSLAC, the magnetic energy decreases with angle when the electronic spin is in the $|-\rangle$ state so the spin misaligns the NV axis from to the B field axis. Driving the $|+\rangle$ to $|-\rangle$ transition in an MDMR means that the particle will then seek large angles. Due to the avoided crossing, larger angles correspond to a larger transition frequency. In the non-linear regime, the MDMR will thus have their sharp edges on the high frequency side of the MDMR peak. This is what is shown in the inset of Fig. 2-b) in the main text where MDMR was performed with 10 averages. Similar measurements are shown in the extended data 2-b) but with a single shot measurement, enabling sharper jumps to be observed.

Angle and librational frequency dependency with laser power and magnetic field The experiment shown in Fig. 2-b) was realized by recording several MDMR. They are shown in the extended data. The magnetic field amplitude was tuned using a permanent magnet held to a motorized translation stage that displaces the magnet position under vacuum. For the experiments shown in Fig. 2-c), the translation stage was positioned on a rotating platform that was actuated by hand. The parameters with the largest uncertainties for these experiments and those presented in Fig. 3 are the number of spins $N \approx 10^9$, the moment of inertia $I \approx 10^{-22} \text{ kg.m}^2$, the Paul trap angular potential depth $U \approx 10^{-16} \text{ J}$, and laser polarization rate which ranges from 10 to 500 kHz depending on the longitudinal T_1 time. The latter depends on the concentration of NV centers, on the so-called “fluctuators” [4] in the diamond as well as on the angle between the B field and the NV axis [5]. Only the angle of the NV axis and the B field are known with high precision thanks to NV magnetometry. Using the mean values of the above parameters and a numerical calculation (see SI) gave agreements by about one order of magnitude with the experimental results that are presented in Fig. 2 and 3. Full numerical fitting using five independent parameters using a three-level model for the spin takes more than one hour on a fast computer. Qualitative agreement could be realized using a mixture between a full 7-level models to derive the density matrix and then an analytical calculation. Analytical solutions can be found only when the angles between the NV and B field axis are less than 1 degrees. It would however require the Paul trap restoring torque to be orders of

magnitude smaller than the spin restoring torque.

Magnetic potential energy The potential energy coming from the electronic spins of the NV centers in the magnetic field are derived by computing the mean of the

torque operators, defined as $\hat{\tau}_\theta = -\frac{\partial H}{\partial \theta}$ for the angle θ and then integrating over the angles θ and ϕ to obtain the potential energy.

- [1] T. Delord, P. Huillery, L. Nicolas, and G. Hétet, *Nature* **580**, 56 (2020).
- [2] M. W. Doherty, N. B. Manson, P. Delaney, F. Jelezko, J. Wrachtrup, and L. C. L. Hollenberg, *Physics Reports* **528**, 1 (2013).
- [3] P. Huillery, J. Leibold, T. Delord, L. Nicolas, J. Achard, A. Tallaire, and G. Hétet, *arXiv e-prints arXiv:2005.13082* (2020), 2005.13082.
- [4] J. Choi, S. Choi, G. Kucsko, P. C. Maurer, B. J. Shields,

- H. Sumiya, S. Onoda, J. Isoya, E. Demler, F. Jelezko, et al., *Phys. Rev. Lett.* **118**, 093601 (2017), ISSN 0031-9007, 1079-7114, number: 9, URL <https://link.aps.org/doi/10.1103/PhysRevLett.118.093601>.
- [5] A. Jarmola, V. M. Acosta, K. Jensen, S. Chemerisov, and D. Budker, *Phys. Rev. Lett.* **108**, 197601 (2012).

SUPPLEMENTARY MATERIAL

In this supplementary material, we provide an analytical treatment of the induced magnetization and of the torque exerted by the spin of the NV centers in the trapped diamond. We will consider the simplified regime of a single NV center whose quantization axis makes a very small angle with the magnetic field. After the GSLAC, the doped-diamond is in the diamagnetic phase, where one of the [111] crystalline diamond directions is aligned to the B field. In this limit, the magnetic field response for that class is an order of magnitude larger than that from the other classes of NV centers who are largely mixed by the transverse magnetic field so this approximation is well-justified.

In the first section, we use perturbation theory by assuming that the spins are prepared in a pure state. Then, we use the von-Neumann equation to evaluate the role of decoherence on the NV centers's spin.

I. MAGNETIC RESPONSE USING PERTURBATION THEORY

In the body fixed frame, the hamiltonian of the electronic spin of a single charged NV center under a magnetic field reads

$$\hat{\mathcal{H}} = \hbar D \hat{S}_{z'}^2 + \hbar \gamma_e \hat{\mathbf{S}} \cdot \mathbf{B}. \quad (3)$$

where $D = (2\pi)2.87\text{GHz}$ is the zero field splitting caused by magnetic dipole-dipole interactions between the two unpaired spins in the ground state of the NV⁻ center spin-triplet. We simplify the problem by assuming that the motion is in the $x - z$ plane and the B field along z , so the magnetic part of the hamiltonian can be written as $\hat{\mathcal{H}}_B = \gamma_e B (-\hat{S}_{x'} \sin \theta + \hat{S}_{z'} \cos \theta)$, where θ is the angle between the B field and NV center quantization axis.

In the $\{|+1\rangle, |0\rangle, |-1\rangle\}$ basis, the hamiltonian of the charged nitrogen-vacancy center's electronic spin reads :

$$\hat{\mathcal{H}} = \hbar \begin{pmatrix} D + \gamma_e B \cos \theta & -\frac{\gamma_e B}{\sqrt{2}} \sin \theta & 0 \\ -\frac{\gamma_e B}{\sqrt{2}} \sin \theta & 0 & -\frac{\gamma_e B}{\sqrt{2}} \sin \theta \\ 0 & -\frac{\gamma_e B}{\sqrt{2}} \sin \theta & D - \gamma_e B \cos \theta \end{pmatrix}_{z'}.$$

A. Close to the GSLAC

Close to the ground state level anti-crossing (GSLAC), where $D - \gamma_e B \ll \gamma_e B$, the energy of the higher lying eigenstate is much greater than that of the other two low lying eigenstates, so it remains an eigenstate of the $\hat{S}_{z'}$ operator to a good approximation. One can thus only consider the subspace formed by the state $|0\rangle$ and $|-1\rangle$ and write the hamiltonian as

$$\hat{\mathcal{H}}_{\text{GSLAC}} = \hbar \begin{pmatrix} 0 & -\frac{\gamma_e B}{\sqrt{2}} \sin \theta \\ -\frac{\gamma_e B}{\sqrt{2}} \sin \theta & D - \gamma_e B \cos \theta \end{pmatrix}_{z'}. \quad (4)$$

The eigenstates of this hamiltonian are

$$|+\rangle = \cos \Psi | -1 \rangle + \sin \Psi | 0 \rangle \quad (5)$$

$$|-\rangle = \cos \Psi | 0 \rangle - \sin \Psi | -1 \rangle \quad (6)$$

where

$$\tan 2\Psi = \frac{2\sqrt{2}\gamma_e B \sin \theta}{D - \gamma_e B \cos \theta} \quad (7)$$

and $2\Psi \in [0, \pi]$. The energies in the states $|+/-\rangle$ of $\hat{\mathcal{H}}_{\text{GLSAC}}$ are plotted in Fig. 6 as a function of B , for an angle $\theta = 0.03$ rad (trace i) and $\theta = 0.0$ rad (trace ii) with respect to the magnetic field.

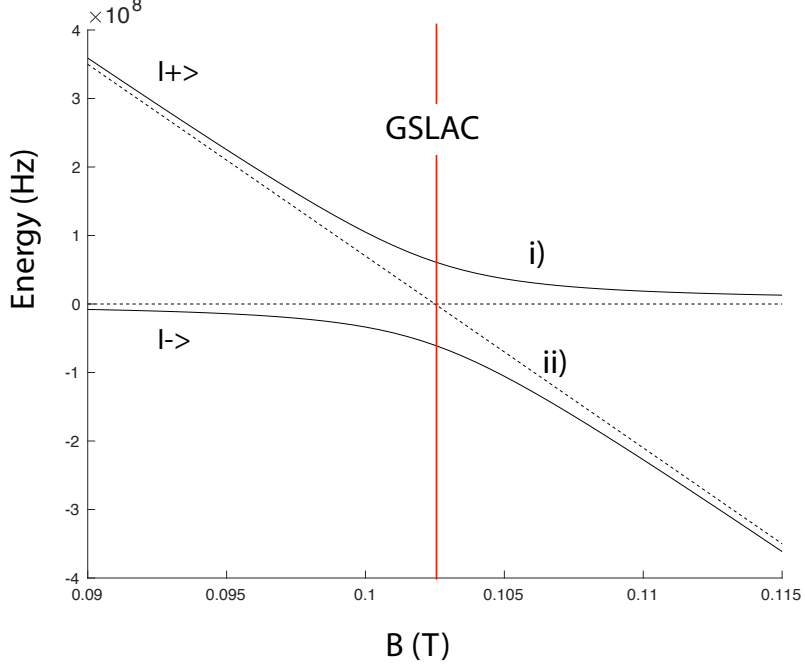


FIG. 6. Energies of the two quasi-resonant states close to the ground state level anti-crossing, with an angle $\theta = 0.03$ rad (trace i), plain lines), at an angle $\theta = 0$ rad (trace ii), dashed lines).

Let us consider mixing angles Ψ close to 0 and $\pi/2$ where the states $|0\rangle$ and $| -1 \rangle$ are only slightly perturbed by the transverse B field. In this so-called dispersive limit, the eigenstates of $\hat{\mathcal{H}}_{\text{GLSAC}}$ are close to being those of $\hat{S}_{z'}$. Note that, due to the intersystem crossing in the optically excited state of the NV center, the state that is populated in the steady state is the state with the largest projection onto the bare $|0\rangle$ state. Before the GSLAC ($D - \gamma_e B \cos \theta > 0$), the NV centers electronic spins are thus mostly in the ground state ($| -1 \rangle$) while, after the GLSAC, the spins are mostly populating the first excited state ($| + \rangle$). As can be seen in the Fig.1, after the GSLAC, the magnetic energy thus increases when the NV deviates from the angle $\theta = 0$ so the electronic spins exert a restoring torque which tends to bring back the NV axis along the B field axis.

We first use second-order perturbation theory to quantify this effect. Assuming $\theta \ll 1$, we can write

$$\hat{\mathcal{H}}_{\text{GSLAC}} = \hbar \begin{pmatrix} 0 & -\frac{\gamma_e B}{\sqrt{2}} \theta \\ -\frac{\gamma_e B}{\sqrt{2}} \theta & \Delta \end{pmatrix}_{z'} = \hbar \begin{pmatrix} 0 & 0 \\ 0 & \Delta \end{pmatrix}_{z'} - \hbar \frac{\gamma_e B \theta}{\sqrt{2}} \begin{pmatrix} 0 & 1 \\ 1 & 0 \end{pmatrix}_{z'} = H_\Delta + V(\theta) \quad (8)$$

where $\Delta = D - \gamma_e B$. In the presence of $V(\theta)$, the perturbed energy ϵ_0 of the state $|0\rangle$ reads

$$\epsilon_0 = \frac{|\langle 0 | V(\theta) | -1 \rangle|^2}{-\hbar \Delta} = -\hbar \frac{(\gamma_e B)^2}{2\Delta} \theta^2 = -\hbar \frac{(\gamma_e B_\perp)^2}{2\Delta} \quad (9)$$

Note that such a change in the magnetic energy in second order perturbation theory is what gives Van-Vleck paramagnetism in many materials. The perturbation V mixes the eigenstates, which induces a magnetization and

a spin-torque. Typically though, spin-orbit coupling is the dominant energy term in the absence of magnetic field. The corresponding splitting is typically many GHz so that it competes with diamagnetism from the electron orbital motion. In the case of the NV center spin-triplet, this energy is given by the magnetic dipole interaction between the two unpaired electrons which is much smaller than typical spin-orbit splittings, and can therefore give a strong induced magnetization close to the GSLAC.

The magnetization M_{\perp}^0 , in the state $|0\rangle$ for one NV center reads

$$M_{\perp}^0 = -\frac{\partial\epsilon_0}{\partial H_{\perp}} = \mu_0\hbar\frac{\gamma_e^2}{\Delta}H_{\perp} \quad (10)$$

The induced magnetization M_{\perp}^0 is opposed to, or is parallel to the applied magnetic field, depending on the sign of Δ . Before the GLSAC, the NV doped-diamond is thus in a paramagnetic regime, while it turns into a diamagnet after the GSLAC. Using the Hellmann-Feynman theorem, one finds the torque in the $|0\rangle$ state to be

$$\langle \hat{\tau} \rangle_0 = -\frac{\partial\epsilon_0}{\partial\theta} = \hbar\frac{(\gamma_e B)^2}{\Delta}\theta \quad (11)$$

In the para- (dia-) magnetic phase, the gradient of the torque with respect to the angle is thus positive (negative) which tends to push (bring) the NV axis away from (close to) the B field.

B. Mechanical detection of the magnetic resonance in the non-linear regime

The above described situation reverses in the presence of a microwave drive on the $|+\rangle$ to $|-\rangle$ transition. We have seen that after the GSLAC, the magnetic energy increases in the stationary state $|+\rangle$ when the angle changes, which provides a restoring torque. Then, if a microwave tone fully populates the $|-\rangle$ state, magnetic energy decreases with angle, so the spin misaligns the NV axis from the B field axis. Driving the $|+\rangle$ to $|-\rangle$ transition with microwave means that the particle will tend to seek large angles.

Because of the avoided crossing, larger angles will correspond to a larger transition frequency. In the non-linear regime where the angular displacement modifies the microwave resonance condition, the mechanically detected magnetic resonances will thus have their sharp edges on the high frequency side of the ESR peak. This is what is observed in the inset of Fig. 2-b) in the main text. This trend is the opposite to when the Paul trap is the dominant cause of angular confinement. Microwave driving to magnetic states tends to pull the angle so that the transition frequencies increase [1], giving rise to a sharp edge on the red side of the mechanically detected ESR.

II. STEADY STATE TORQUE CLOSE TO THE GSLAC

We now analyse the effects of dissipation in the magnetization and the spin-torque.

The von Neumann Master equation for the density matrix reads

$$\frac{d\hat{\rho}}{dt} = -\frac{i}{\hbar}[\hat{\mathcal{H}}, \hat{\rho}] + \mathcal{L}(\hat{\rho}) \quad (12)$$

$\mathcal{L}(\hat{\rho})$ describes longitudinal relaxation of the spin population at a rate Γ_1 , optical pumping from the $m_s = \pm 1$ to the $m_s = 0$ state at a rate γ_{las} as well as pure dephasing of all the states at a rate Γ_2^* .

We have

$$\hat{\rho} = \begin{pmatrix} \rho_{11} & \rho_{10} & \rho_{1-1} \\ \rho_{10}^* & \rho_{00} & \rho_{0-1} \\ \rho_{1-1}^* & \rho_{0-1}^* & \rho_{-1-1} \end{pmatrix}_{z'}.$$

A. Density matrix in the steady state

We will again consider that the magnetic field satisfies $D - \gamma_e B \ll \gamma_e B$, so the B field brings the two ground states close to the GLSAC. The $+1$ state energy thus always lies far from the energy of the two other states $|0\rangle, | -1 \rangle$. Let

us then neglect coherences between $|+1\rangle$ and the other states $| -1 \rangle, | 0 \rangle$. We thus assume that $\rho_{-11}, \rho_{01} \ll \rho_{-10}$. We have

$$-\frac{i}{\hbar}[\hat{\mathcal{H}}, \hat{\rho}] = -i \begin{pmatrix} 0 & * & * \\ * & -\frac{\gamma_e B}{\sqrt{2}} \sin \theta (\rho_{0-1}^* - \rho_{0-1}) & -\frac{\gamma_e B}{\sqrt{2}} \sin \theta (\rho_{-1-1} - \rho_{00}) - (D - \gamma_e B \cos \theta) \rho_{0-1} \\ * & -\frac{\gamma_e B}{\sqrt{2}} \sin \theta (\rho_{00} - \rho_{-1-1}) + (D - \gamma_e B \cos \theta) \rho_{0-1}^* & +\frac{\gamma_e B}{\sqrt{2}} \sin \theta (\rho_{0-1}^* - \rho_{0-1}) \end{pmatrix}_{z'}, \quad (13)$$

so that in the steady state:

$$0 = -\Gamma_1(\rho_{11} - \rho_{00}) - \gamma_{\text{las}} \rho_{11} \quad (14)$$

$$0 = -i \frac{\gamma_e B}{\sqrt{2}} \sin \theta (\rho_{0-1}^* - \rho_{0-1}) - \Gamma_1(\rho_{-1-1} - \rho_{00}) - \gamma_{\text{las}} \rho_{-1-1} \quad (15)$$

$$0 = -i \left(-\frac{\gamma_e B}{\sqrt{2}} \sin \theta (\rho_{-1-1} - \rho_{00}) - (D - \gamma_e B \cos \theta) \rho_{0-1} \right) - \Gamma_2^* \rho_{0-1} \quad (16)$$

$$1 = \rho_{11} + \rho_{00} + \rho_{-1-1}. \quad (17)$$

Solving this equation, we obtain

$$\rho_{0-1} = -\frac{\frac{\gamma_e B}{\sqrt{2}} \sin \theta}{(D - \gamma_e B \cos \theta) + i\Gamma_2^*} (\rho_{-1-1} - \rho_{00}), \quad (18)$$

and then

$$\rho_{-1-1} = \frac{\Gamma_m(\theta) + \Gamma_1}{3\Gamma_1 + \gamma_{\text{las}} + 2\Gamma_m(\theta)(1 + \frac{\Gamma_1/2}{\Gamma_1 + \gamma_{\text{las}}})}, \quad (19)$$

and

$$\rho_{00} = \frac{\Gamma_m(\theta) + \Gamma_1 + \gamma_{\text{las}}}{3\Gamma_1 + \gamma_{\text{las}} + 2\Gamma_m(\theta)(1 + \frac{\Gamma_1/2}{\Gamma_1 + \gamma_{\text{las}}})}, \quad (20)$$

where

$$\Gamma_m(\theta) = \frac{1}{2} \frac{\Gamma_2^* (\gamma_e B)^2 \sin^2 \theta}{(D - \gamma_e B \cos \theta)^2 + \Gamma_2^{*2}} \quad (21)$$

is the mixing rate due to the magnetic field angle with respect to the $<111>$ direction.

Full numerical solutions in fact suggest that for angle above 0.01 radians, the assumption $\rho_{01} \ll \rho_{-10}$ is no longer correct. The above analytical solutions apply only for a very small angle range. In the experiments, the minimal angle that was achieved is 2.5 degrees (or 0.05 radians) where this analytical theory would only give partial qualitative with the experiment.

B. Spin-torque close to the GLSAC

The spin adiabatically follows the change in the diamond angle. The mean value of the torque in terms of the reduced density matrix elements ρ_{ij} in the basis of the three $\hat{S}_{z'}$ eigenstates $\{|0\rangle_{z'}, |\pm 1\rangle_{z'}\}$ is then

$$\langle \hat{\tau} \rangle = \hbar \gamma_e B (\rho_{-1-1} - \rho_{11}) \sin \theta - \hbar \frac{\gamma_e B}{\sqrt{2}} S \cos \theta, \quad (22)$$

where we introduced the scalar $S = \rho_{0,1} + \rho_{1,0} + \rho_{0,-1} + \rho_{-1,0}$.

With the above restrictions in mind, let us compute the torque when the angle is below 0.01 radians. Plugging Eq. (18) into Eq. (22), we get

$$\langle \hat{\tau} \rangle = \hbar \frac{(\gamma_e B)^2 \Delta}{\Delta^2 + \Gamma_2^{*2}} \left(\frac{\gamma_{\text{las}}}{3\Gamma_1 + \gamma_{\text{las}}} \right) \frac{1}{1 + \frac{\Gamma_m(\theta)}{\Gamma_1 + \gamma_{\text{las}}}} \frac{\sin 2\theta}{2}. \quad (23)$$

where $\Delta = D - \gamma_e B$. We have made the replacement $\cos \theta \approx 1$ and $\sin \theta \approx \theta$. For a sufficiently strong laser such that $\Gamma_m(\theta) \ll \gamma_{\text{las}}$, we get

$$\langle \hat{\tau} \rangle = \hbar \frac{(\gamma_e B)^2 \Delta}{\Delta^2 + \Gamma_2^{*2}} \frac{\gamma_{\text{las}}}{3\Gamma_1 + \gamma_{\text{las}}} \theta, \quad (24)$$

The torque is thus a linear function of the angle in the small angle region. The spin-torque will thus be anti-confining for $\gamma_e B < D$ (paramagnetic regime) and confining for $\gamma_e B > D$ (diamagnetic regime). In the limit where $\gamma_{\text{las}} \gg \Gamma_1$ and $\Delta \gg \Gamma_2^*$, we recover the expression given by Eq. (11) that was obtained from perturbation theory.

One can estimate the librational frequency in our experimental conditions (where $\Delta \gg \Gamma_2^*$) to be

$$\omega_\theta = \sqrt{\frac{\hbar}{I\Delta} \frac{\gamma_{\text{las}}}{3\Gamma_1 + \gamma_{\text{las}}} \gamma_e B}. \quad (25)$$

ω_θ is thus proportional to the magnetic field, as expected for induced magnetic processes such as para/dia-magnetism.

To obtain the torque for many spins we simply multiply the torque by the number of spins N . Taking $B \approx 0.2$ T and $N = 10^9$ fully polarized spins in a $15\mu\text{m}$ diamond with a moment of inertia $I \approx 10^{-22}$ kg.m 2 , we obtain $\frac{\omega_\theta}{2\pi} \approx 2$ kHz, which is greater than the typical Paul trap frequencies, which range from 100 to 1 kHz. The above calculations describe the para/dia transition and the resulting confinement in the diamagnetic regime but cannot be used *in extenso* to fit our experiments. Because of the Paul trap restoring force, the angle between the NV centers and magnetic field is indeed, at best, 2.5 degrees, so the theory must be modified to include all three levels.

[1] T. Delord, P. Huillery, L. Nicolas, and G. Hétet, *Nature* **580**, 56 (2020).